15th Australasian Fluid Mechanics Conference
The University of Sydney, Sydney, Australia
13-17 December 2004

Convective Exchange between two Connected Chambers

M. A. Coman, G. O. Hughes and R. C. Kerr

Research School of Earth Sciences
The Australian National University, Canberra ACT 0200, AUSTRALIA

Abstract

High Rayleigh number convection is studied experimentally in a differentially heated cavity that consists of two connected chambers. We investigate how the circulation, the temperature field and the transport of heat and mass depend on the height of the barrier separating the chambers. We find that the temperature fields in the chambers are very different and that a complex flow structure evolves to accommodate the heat and mass transports. Surprisingly, both of these transports are found to have little dependence on the barrier height, and only begin to decrease rapidly when the barrier height becomes very large.

Introduction

Convection in a two-dimensional differentially heated cavity has been extensively studied, motivated by a wide range of engineering applications [1, 2, 3, 4, 7]. At high Rayleigh numbers, a strong boundary layer circulation (figure 1) accommodates most of the mass and heat fluxes: a buoyant plume rises up the heated endwall, flows along the top of the cavity, falls down the cooled endwall as a dense plume, and then returns along the bottom of the cavity [2, 3, 4]. Fluid in the cavity interior or 'core' is nearly stagnant and has a temperature field that varies linearly with depth and is independent of longitudinal position [1, 7].

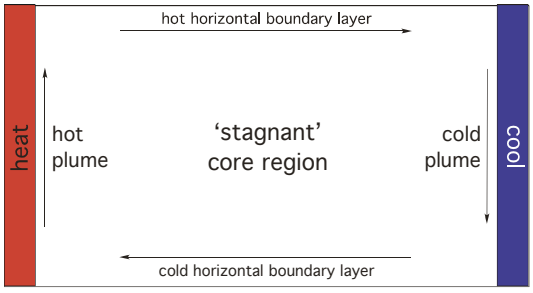

Figure 1: Schematic of the boundary layer circulation in a differentially heated cavity at high Rayleigh number (no barrier).

In many geophysical, environmental and industrial situations convective circulation is strongly influenced by complex bottom topographies or building geometries [5, 6, 8]. As a step towards understanding these more complex flows, we have placed a barrier in the cavity interior that blocks the boundary layer circulation and changes the flow significantly. In this paper we describe how the flow changes as a function of barrier height and present measurements of the modified heat and mass transports in the cavity.

Experimental Apparatus & Methods

The experimental set-up is illustrated in figure 2. The experiments were carried out in a tank of length L = 302 mm, height H = 196 mm and width W = 150 mm. The base, lid and sidewalls were made of Perspex, with heat exchangers as endwalls. Each heat exchanger was kept at a constant temperature by recirculating water from a temperature-controlled bath. The temperature in the heat exchangers was monitored using embedded thermistors. Water was used as the working fluid in the tank. Four holes along the length of the tank in the centre of the lid accommodated flow visualisation and temperature measurements. This ensured all visualisation and measurements were subject to minimal influence from the sidewalls. Barriers of the same width as the tank and of height h = 36 mm, 56 mm, 76 mm, 96 mm, 116 mm, 136 mm, 156 mm and 176 mm, were inserted half way along the tank at the bottom so as to create two connected chambers of equal size. The barriers were made of 20 mm thick Styrofoam with rubber sealing on the three sides touching the tank to ensure minimal conductive heat transfer and no water leakage between chambers. Heat loss from the tank was minimised by double glazed Perspex sidewalls. In addition, the tank was insulated on all sides with Styrofoam. The insulation on the two sidewalls was removed only when photos and temperature profiles were being collected. The heat loss from the tank was found to be minimal, about 1% of the total convective heat flux in the no barrier case.

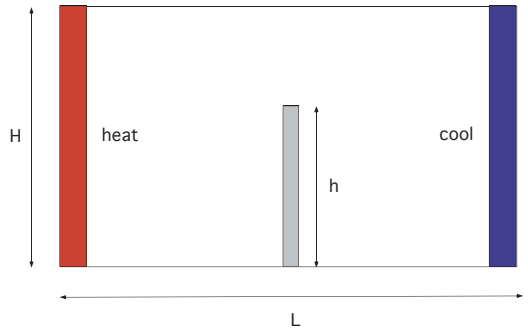

Figure 2: Experimental configuration (elevation view).

In each experiment the tank was carefully filled using de-aired water to reduce the amount of bubbles present. Two free standing thermistors were placed in the interior of the tank, one in the middle of each chamber. Temperatures were logged on a PC and when the readings from all the thermistors were constant (after typically 15 hours), the system was considered to have reached thermal equilibrium.

Once at equilibrium, temperature profiles through the two chambers and through the depth above the barrier were measured. Potassium permanganate crystals and food dye were introduced into the flow through the holes in the tank lid. A slide projector was placed a few metres behind the tank illuminating a sheet of tracing paper attached to the back of the tank. The tracing paper acted as a light diffusing screen, against which the dye could be easily seen. A Nikon D100 digital camera was used to take photos during the experiments. Horizontal velocity measurements were made in the centre of the tank, above the barrier, in order to determine the mass and heat fluxes in the flow. Approximately vertical dyelines were generated by dropping potassium permanganate crystals through the flow. Pho-

tographs were taken at intervals between two and sixty seconds, and the velocities calculated (with an accuracy of $\pm 5\%$) using the horizontal displacement in dye line positions from one photo to the next.

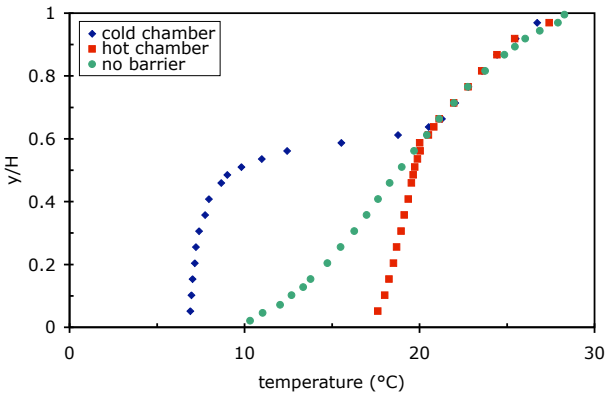

Figure 3: Steady-state temperature profiles through the two chambers for $A_B = 0.59$. The steady-state temperature profile at the centre of the tank for the flow with no barrier is also shown.

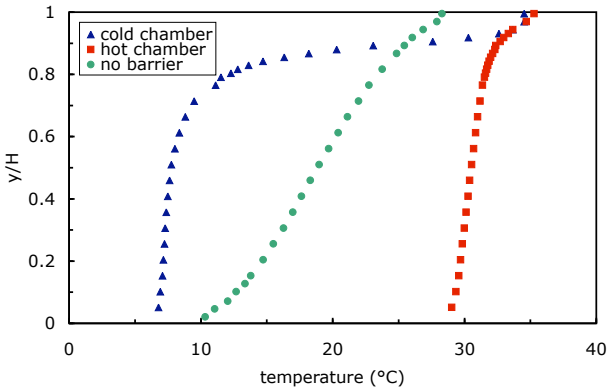

Figure 4: Steady-state temperature profiles through the two chambers for $A_B = 0.90$. The steady-state temperature profile at the centre of the tank for the flow with no barrier is also shown.

In this flow there are four important parameters: the Rayleigh number

$$Ra = \frac{\alpha g \Delta T H^3}{\nu \kappa} = 5 \times 10^9, \tag{1}$$

the Prandtl number

$$Pr = \frac{\nu}{\kappa} = 7, \tag{2}$$

the aspect ratio

$$A = \frac{H}{L} = 0.65, \tag{3}$$

and the barrier aspect ratio

$$A_B = \frac{h}{H}, \tag{4}$$

where g is the gravitational acceleration, α is the expansion coefficient, ΔT is the applied temperature difference between the two endwalls, ν is the kinematic viscosity and κ is the thermal diffusivity.

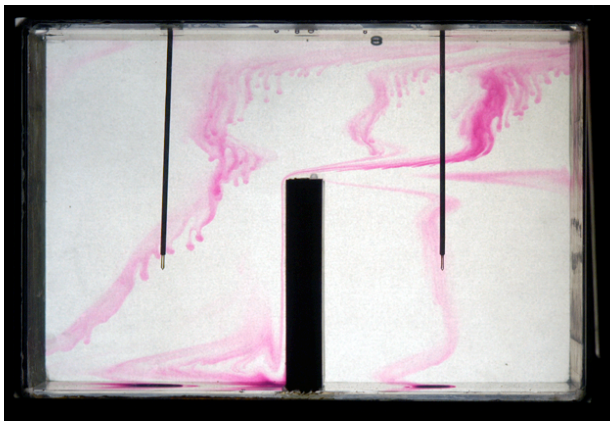

Figure 5: Visualisation of the flow for $A_B = 0.59$. Initially vertical dye streaks were generated by dropping potassium permanganate crystals at three positions: the centre of the tank and aligned horizontally with the thermistors (visible in the centre of each chamber).

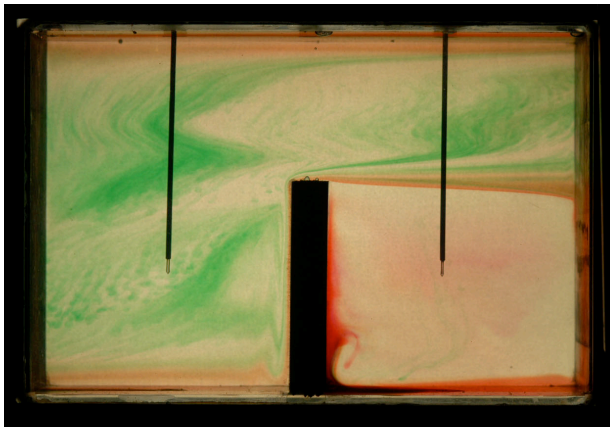

Figure 6: Visualisation of the flow for $A_B = 0.59$. Red dye was introduced into the boundary layer at the bottom of each chamber and at a later time green dye was added to the interior of the tank.

In this paper only A_B is varied, by changing the barrier height h. The other parameters are fixed as we are using the same tank, keeping water as the working fluid, and using an applied temperature difference $\Delta T = 45\,^\circ$C (the heated endwall had a temperature $T_{hot} = 50\,^\circ$C and the cooled endwall had a temperature $T_{cold} = 5\,^\circ$C).

Qualitative Observations

When a barrier is inserted into the cavity, fluid in the cold horizontal boundary layer in figure 1 is prevented from flowing all the way to the hot plume. Instead the outflow from the cold plume pools and slowly fills the right chamber in figure 2. Eventually, the coldest water totally fills this chamber to the height of the barrier, creating a 'cold chamber' whose final steady-state temperature profile contrasts dramatically with the temperature profile in the adjacent 'hot chamber' (see figures 3 and 4). The presence of a barrier has a significant effect on the temperature profile at the uppermost levels in the tank only when the gap above the barrier is small (compare figures 3 and 4).

Figures 5 and 6 show visualisations of the steady state circulation for $A_B = 0.59$. The hot plume (not visible) rises up the heated endwall and detrains to form the hot horizontal boundary layer. The cold plume forms at the top of the cooled endwall and flows down the plate, but splits into two at around the height of the barrier. The coldest fluid from the inner part of the plume (against the endwall) continues to flow downwards, but the fluid in the outer part of the plume is not cold enough to penetrate into the cold chamber: it instead detrains and flows horizontally towards the barrier. Along the way, the intruding flow is combined with upwelling fluid from the cold chamber to produce a strongly stratified overflow at the barrier (see figure 8). This flow then plunges over the side of the barrier forming a fast downflowing plume. In a manner very similar to a plume entering a stratified environment, the momentum of the downflowing fluid causes it to overshoot and then oscillate about its level of neutral buoyancy in the heated chamber (figures 5 and 6). As the overflow is strongly stratified, only the very coldest fluid immediately adjacent to the barrier is observed to reach the tank bottom, while the remainder enters the interior of the heated chamber at a range of different levels (figures 5 and 6). This fluid is then gradually drawn towards the lower part of the heated endwall, where it is entrained into the hot plume.

In the cold chamber, the flow is primarily driven by the cold sidewall plume, which produces a slow upwelling return flow (figure 6). The cold chamber is also weakly stirred by a small amount of heat transfer through the barrier (less than 3% of the total amount).

Quantitative Results

The exchange flow above the barrier was found to be strongly dependent on the barrier height (see figure 7). In the no barrier case (figure 7 a), we observed strong boundary layer flows at the top and bottom, with a weak uniform shear in the interior (cf. figure 1). With the addition of a small barrier (figure 7 b), the top half of the flow is similar to the no barrier case (figure 7 a), but the bottom half is significantly different: the return flow occurs in a thinner layer with a much faster velocity. This barrier overflow also generates horizontal shear layers in the overlying fluid (cf. [9]), which are identified by a local maximum or minimum in the velocity profile. As h is increased, the region of uniform shear in the interior steadily decreases until it disappears at $A_B = 0.59$ (figure 7 c). When h is increased further, the number of shear layers decreases from six (for $A_B = 0.59$) to four (for $A_B = 0.59$, see figure 7 d), and then to a simple bi-directional exchange flow for the highest barrier (figure 7 e), where a layer of warm water flowing towards the cooled endwall overlies a cooler layer overflowing the barrier.

In figure 8, the temperature profile above the barrier is shown for a number of different barrier heights. As the barrier height is increased, two main effects are observed. First, the temperature gradient in the barrier overflow systematically increases. Second, the temperature profiles are shifted to warmer temperatures. However, the temperature gradient above the barrier appears to be unchanged (cf. figures 3 and 4).

From integration of the velocity profiles in figure 7, we determined the volume flow per unit width from the hot chamber to the cold chamber, as a function of the barrier height (figure 9). The volume flow was expected to decrease steadily with increasing barrier height. However, for modest barrier heights, no such decrease was observed (and there is a suggestion of a maximum in flow rate at around $A_B \sim 0.4$). A substantial decrease in volume flow was only apparent when the barrier height became very large ($A_B > 0.8$), which satisfies the constraint that the volume flow must go to zero as $h \to H$ (and the gap closes).

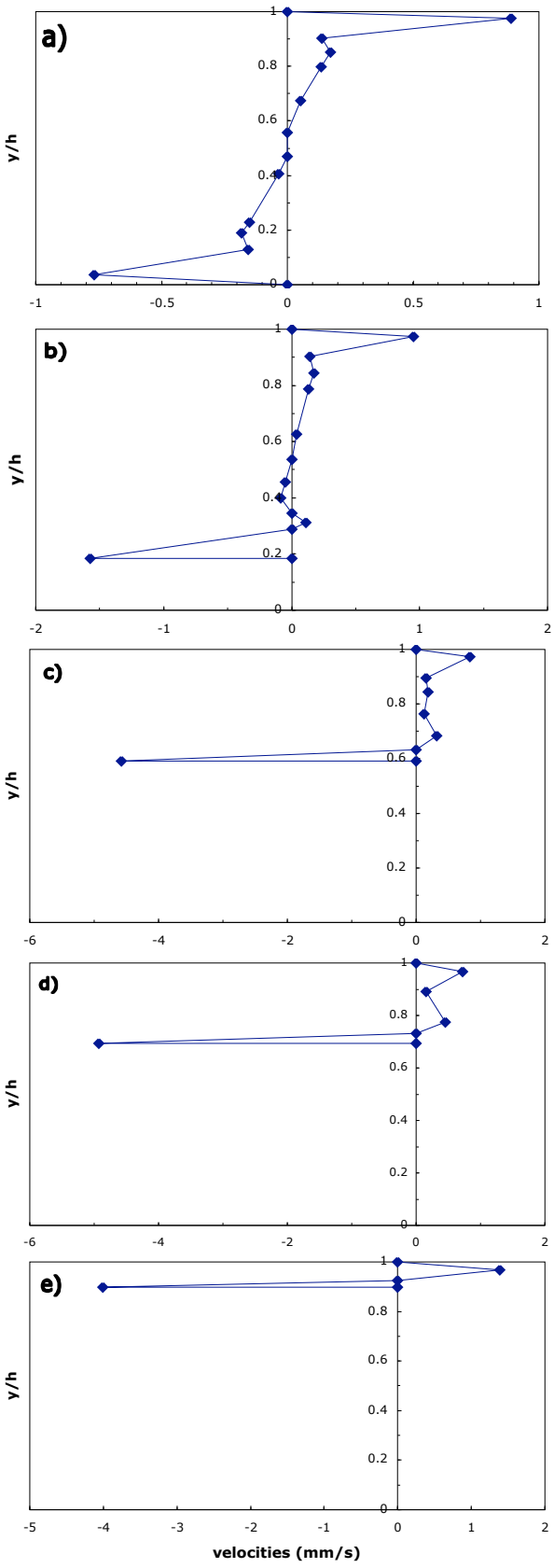

Figure 7: Velocity profiles above the barrier for a) $A_B = 0$, b) $A_B = 0.18$, c) $A_B = 0.59$, d) $A_B = 0.69$, e) $A_B = 0.90$. The points on the plots in (c) – (e) correspond to heights at which the velocity was either zero or a local maximum/minimum. Note that the horizontal scale differs for each plot.

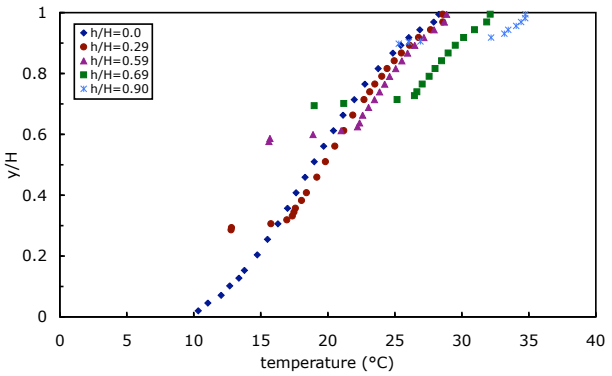

Figure 8: Temperature profiles above the barrier for $A_B = 0$, 0.29, 0.59, 0.69, 0.90.

From the measured velocity and temperature profiles, we determined the heat transport per unit width q across the barrier

$$q = \rho c_p \int_h^H uT\,dy, \tag{5}$$

where ρ is the density, y is the vertical coordinate and c_p is the specific heat of water at constant temperature. The Nusselt number is then given by

$$Nu = \frac{q}{k\Delta T} \tag{6}$$

where k is the thermal conductivity of water. The measured Nusselt numbers are plotted in figure 10 as a function of barrier height. We had anticipated that the heat transport would steadily decrease with increasing barrier height. However, no decrease was observed for modest barrier heights, and a rapid decrease in heat transport was found when $A_B > 0.8$ (satisfying the constraint that the heat transport must go to zero as $h \to H$).

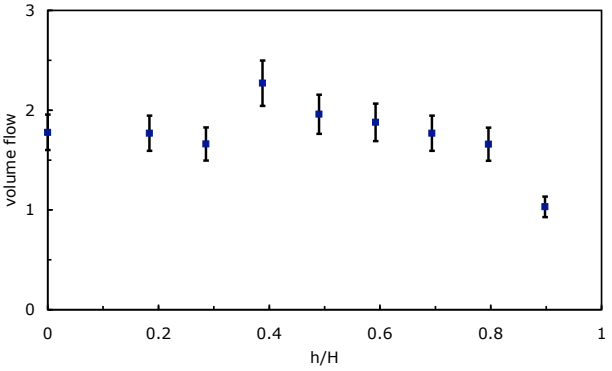

Figure 9: Volume flow per unit width (in $10^{-5}\,\mathrm{m}^2/\mathrm{s}$) exchanged through the gap above the barrier as a function of A_B.

Conclusions

We have studied the convective flow in two connected chambers by placing a partial-height barrier into a cavity with differentially heated endwalls. The introduction of the barrier severely disrupts the transport of heat and mass in the boundary layers and plumes adjacent to the cavity walls. Temperature profiles in the cavity are dramatically modified, with the formation of a very cold chamber and a moderately warmer chamber. An unexpected flow structure arises to accommodate the exchange

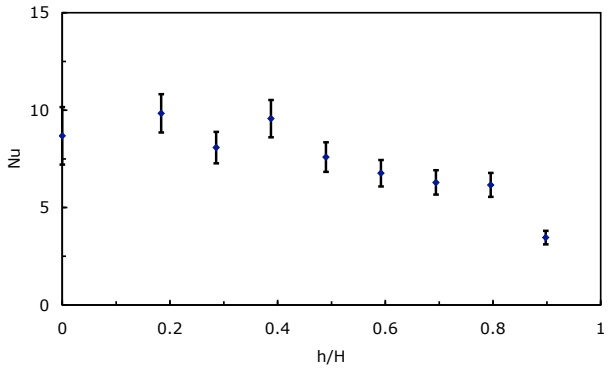

Figure 10: Measured Nusselt number as a function of A_B.

of fluid between the chambers. Contrary to intuition the heat and mass transport is little changed by the presence of a moderate barrier, and only begin to decrease rapidly when the barrier height becomes very large (when $A_B > 0.8$). The complex dynamics responsible for this behaviour are currently being studied.

Acknowledgements

Technical assistance from Tony Beasley and Brad Ferguson is gratefully acknowledged. We also thank Ross Griffiths for help throughout this project.

References

[1] Bejan, A., Al-Homoud, A. A. and Imberger, J., Experimental study of high-Rayleigh number convection in a horizontal cavity with different end temperatures, *J. Fluid Mech.*, **109**, 1981, 283-299.

[2] Bejan, A. and Tien, C. L., Laminar Natural Convection Heat Transfer in a Horizontal Cavity with Different End Temperatures, *J. Heat Transfer*, **100**, 1978, 641-647.

[3] Cormack, D.E., Leal, L. G and Seinfeld J. H., Natural convection in a shallow cavity with differentially heated end walls. Part 2, *J. Fluid Mech.*, **65**, 1974, 229-246.

[4] Imberger, J., Natural convection in a shallow cavity with differentially heated end walls. Part 3, *J. Fluid Mech.*, **65**, 1974, 247-260.

[5] Linden, P. F., The fluid mechanics of natural ventilation, *Annu. Rev. Fluid Mech.*, **31**, 1999, 201-238.

[6] Lin, Y. J. P. and Linden, P. F., Buoyancy-driven ventilation between two chambers, *J. Fluid Mech.*, **463**, 2002, 293-312.

[7] Simpkins, P. G. and Chen, K. S., Convection in horizontal cavities, *J. Fluid Mech.*, **166**, 1986, 21-39.

[8] Wong, A. B. D. and Griffiths, R. W., Two-basin filling boxes, *J. Geophys Res.*, **106**, 2001, 26929-26941.

[9] Wong, A. B. D., Griffiths, R. W. and Hughes, G. O., Shear layers driven by turbulent plumes, *J. Fluid Mech.*, **434**, 2001, 209-241.